JVI Accepts, published online ahead of print on 20 August 2014
J. Virol. doi:10.1128/JVI.02138-14

The ER stress sensor IRE1α protects cells from apoptosis induced by coronavirus infectious bronchitis virus

To Sing Fung, Ying Liao and Ding Xiang Liu*

School of Biological Sciences, Nanyang Technological University, 60 Nanyang Drive, Singapore 637551

Running Title: Activation of the IRE1-XBP1 pathway by IBV

To whom correspondence should be addressed: Ding Xiang Liu, School of Biological Sciences, Nanyang Technological University, 60 Nanyang Drive, Singapore 637551, Tel:(65) 63162862; Fax: (65) 67913856; E-mail: dxliu@ntu.edu.sg

Abstract

The unfolded protein response (UPR) is a signal transduction cascade triggered by perturbation of the homeostasis of the endoplasmic reticulum (ER). UPR resolves ER stress by activating a cascade of cellular response including the induction of molecular chaperones, translational attenuation, ER-associated degradation and other mechanisms. Under prolonged and irremediable ER stress, however, UPR can also trigger apoptosis. Here we report that in cells infected with the avian coronavirus infectious bronchitis virus (IBV), ER stress was induced and the IRE1α-XBP1 pathway of UPR was activated. Knockdown and over-expression experiments demonstrated that IRE1α protects the infected cells from IBV-induced apoptosis, which required both its kinase and RNase activity. Our data also suggest that splicing of XBP1 mRNA by IRE1α appears to convert XBP1 from a pro-apoptotic XBP1u protein to a pro-survival XBP1s protein. Moreover, IRE1α antagonized IBV-induced apoptosis by modulating the phosphorylation status of the pro-apoptotic c-Jun N-terminal kinase (JNK) and the pro-survival RAC-alpha serine/threonine-protein kinase (Akt). Taken together, the ER stress sensor IRE1α is activated in IBV-infected cells and serves as a survival factor during coronavirus infection.

Importance

Animal coronaviruses are important veterinary viruses, which could cross the species barrier, becoming severe human pathogens. Molecular characterization of the interactions between coronaviruses and host cells is pivotal to the understanding of pathogenicity and species specificity of coronavirus infection. It has been well established that the endoplasmic reticulum (ER) is closely associated with coronavirus replication. Here we report that inositol-requiring protein-1 alpha (IRE1α), a key sensor of ER stress, is activated in cells infected with avian coronavirus infectious bronchitis virus (IBV). Moreover, IRE1α is shown to protect the infected cells from apoptosis by modulating the unfolded protein response (UPR) and two kinases related to cell survival. This study demonstrates that UPR activation constitutes a major aspect of coronavirus-host interactions. Manipulations of the coronavirus-induced UPR may provide novel therapeutic targets to the control of coronavirus infection and pathogenesis.

Introduction

In eukaryotic cells, the endoplasmic reticulum (ER) is the major site where secreted and transmembrane proteins are synthesized and folded. When excessive proteins enter the ER, unfolded proteins accumulate in the ER lumen and cause ER stress. To maintain homeostasis, signaling pathways collectively known as the unfolded protein response (UPR) are activated (1). To date, three UPR sensors have been identified, namely PKR-like ER protein kinase (PERK), activating transcriptional factor-6 (ATF6) and inositol-requiring protein-1 alpha (IRE1α). Activated PERK phosphorylates the α subunit of eukaryotic initiation factor 2 (eIF2α) and results in a global shutdown of protein synthesis to reduce the protein flux into the ER (2). Activated ATF6 is cleaved twice to release a cytosolic fragment, which translocates to the nucleus and transactivates ER protein chaperones that enhance the ER folding capacity (3, 4).

The IRE1α-XBP1 branch of the UPR is evolutionarily conserved from yeast to humans. In response to unfolded proteins, IRE1α dissociates from ER protein chaperones and undergoes oligomerization (5). This results in the autophosphorylation of the kinase domain and activation of the RNase domain. The best characterized substrate for the RNase domain is mRNA of the X box binding protein 1 (XBP1) (6, 7). IRE1α removes a 26-nubleotide intron from XBP1 mRNA to form a frame shift transcript, the spliced XBP1 (XBP1s). While the unspliced XBP1 (XBP1u) mRNA encodes an inhibitor of the UPR, XBP1s encodes a potent transcription activator, which translocates to the nucleus and enhances the expression of many UPR genes, including those encoding molecular chaperones and proteins contributing to ER-associated degradation (ERAD) (8, 9).

If ER homeostasis is not re-established, the UPR can induce apoptosis to eliminate the overly stressed cells. Apoptosis is a highly controlled mode of cell death characterized by cell shrinkage, plasma membrane blebbing and nuclear fragmentation (10). Previously, ER stress-induced apoptosis has been mainly attributed to the induction of C/EBP homologous protein (CHOP) (11). Recently, it has been demonstrated that the IRE1α branch is also involved in regulation of ER stress-induced apoptosis. Activated IRE1α has been found to be associated with TNF receptor-associated factor 2

(TRAF2). This complex further recruits apoptosis-signal-regulating kinase 1 (ASK1), which induces apoptosis by activating the mitogen-activated protein (MAP) kinase JNK (12). In another study, IRE1α has been shown to promote clustering and activation of pro-caspase 12, which subsequently cleaves caspase 3 and induces apoptosis (13, 14).

Coronaviruses are enveloped virus with a large single-stranded, positive-sense RNA genome. Infectious bronchitis virus (IBV) is an avian gammacoronavirus that causes respiratory disease in chickens, resulting in major economic burden to the poultry industry worldwide. During coronavirus infection, tremendous amount of viral proteins are synthesized in the ER. Moreover, the replication and transcription complexes (RTCs) where coronavirus RNA synthesis occurs are originated from a reticular network of modified ER membranes (15, 16). The overloading of ER folding capacity and extensive rearrangement of the ER membrane may cause ER stress and induce UPR, as previously demonstrated in cells infected with mouse hepatitis virus (MHV) (17). Moreover, the envelope protein of severe acute respiratory syndrome coronavirus (SARS-CoV) has been shown to counteract the IRE1α-XBP1 pathway of UPR and inhibit SARS-CoV-induced apoptosis (18). However, the significance of UPR in coronavirus-host interaction remains largely unexplored.

Previously, we have shown that IBV induces apoptosis in late stage infected cells and identified two Bcl-2 family proteins that modulate IBV-induced apoptosis (19-22). However, the mechanisms regulating this process remain largely unexplored. In this study, we focus on the UPR sensor IRE1α and its function in IBV-induced apoptosis. It was found that IBV induced ER stress in infected cells and activated the IRE1α-XBP1 pathway at late stage of infection. Knockdown and over-expression studies showed that IRE1α protected infected cells from IBV-induced apoptosis, which required both the kinase and RNase domains of IRE1α. Splicing of XBP1by IRE1α appears to convert it from a pro-apoptotic unspliced form to an anti-apoptotic spliced form. Moreover, phosphorylation of the pro-apoptotic kinase JNK and the pro-survival kinase Akt was also modulated by IRE1α to promote cell survival during IBV infection. Taken together, our data demonstrate the important pro-survival function of the UPR sensor IRE1α during coronavirus infection.

Materials and methods

Virus and cell lines

The egg-adapted Beaudette strain of IBV (ATCC VR-22) was obtained from American Type Culture Collection (ATCC) and adapted to Vero cells as described (23). To prepare virus stock, monolayers of Vero cells were infected at a multiplicity of infection (MOI) of approximately 0.1 and cultured in plain Dulbecco modified Eagle medium (DMEM) at 37^{o}C for 24 hours. After three freeze/thaw cycles, the cell lysate was clarified by centrifugation at 1,500 g at 4^{o}C for 30 minutes. The supernatant was aliquot and stored at -80^{o}C as virus stock. The titer of the virus preparation was determined by plaque assays. Mock cell lysate was prepared by same treatment of uninfected Vero cells.

Inactivation of IBV was performed by exposing the virus stock to 120,000 mJ/cm^2 of 254-nm shortwave UV radiation for 15 minutes with a CL-1000 cross-linker (UVP) (24). To demonstrate that IBV had been inactivated, Vero cells were incubated with UV-IBV and the cell lysates were analyzed by Western blot to confirm that no viral proteins can be detected.

H1299 cells were cultured in RPMI 1640 medium supplemented with 5% fetal bovine serum (FBS) and 1% Penicillin-Streptomycin (Gibco). All cells were grown in a 37^{o}C incubator supplied with 5% CO_2. In all the experiments, cells were washed twice with PBS before infected with IBV at an MOI of approximately 2 or incubated with equal volume of UV-IBV in serum-free medium. After 2 hours of absorption, cells were washed twice with serum-free medium and kept incubated at 37^{o}C before harvested.

Antibodies, chemicals and reagents

The antibodies against IRE1α (#3294), PARP (#9532), caspase-3 (#9662), caspase-8 (#9746), caspase-9 (#9502), JNK (#9258), phospho-JNK (#4668), Akt (#4691) and phospho-Akt (#4060) were purchased from Cell Signaling Technology. The antibody against enhanced green fluoresence protein was from Sigma. The antibody against β-actin (sc-1616) was from Santa Cruz Biotechnology.

The anti-serum against IBV S protein and N protein were from rabbits immunized with bacterial expressed fusion proteins as previously described (25, 26).

Dithiothreitol (DTT) was purchased from Sigma. The 1 M DTT stock was prepared by dissolving in autoclaved water and stored at -20 ^{o}C. To induce ER stress, cells were treated with 2 mM DTT for 2 hours before harvested for RNA extraction.

Plasmid constructions and transfection

The cDNA of human IRE1α (RefSeq NM_001433.3) was amplified from total RNA of H1299 cells by reverse transcriptase-PCR (RT-PCR) using IRE1α specific primers (forward primer: 5'-CGGGAATTCGGCCGAGTCCTCGCCATG-3', reverse primer: 5'-CAAGCGGCCGCCTTTCCCAACTATCACCACGCT-3'). The PCR product was digested with *EcoRI* and *NotI* and inserted to *pHA-C*, which has a HA-tag coding sequence inserted between the *NotI* and *XbaI* site in the parental construct *pcDNA3.1* (Invitrogen). The resulting plasmid was named *pcDNA3.1-IRE1α-HA*. The kinase dead mutant K599A was generated using site-directed mutagenesis (forward primer: 5'- GACGTGGCCGTGGCGAGGATCCTCCCC-3', reverse primer: 5'- GGGGAGGATCCTCGCCACGGCCACGTC-3', mutated nucleotides underlined). The RNase deleted mutant was generated by amplifying DNA fragment from *pcDNA3.1-IRE1α-HA* using specific primers (forward primer 5'- CGGGAATTCGGCCGAGTCCTCGCCATG-3', reverse primer CAAGCGGCCGCCTTTCCCAACTATCACCACGCT) and ligating into the same sites. The cDNA of human XBP1, unspliced isoform (RefSeq NM_005080.3) was amplified from total RNA of H1299 cells by RT-PCR using XBP1u specific primers (forward primer: 5'-GGA***AGATCT***GGAGCTATGGTGGTG-3', reverse primer: 5'-CGG***GGTACC***TTAGTTCATTAATGGCTTCCAGC-3'). The cDNA of human XBP1, spliced isoform (RefSeq NM_001079539.1) was amplified from total RNA of H1299 cells treated with 2 mM DTT for 2 h, using XBP1s specific primers (forward primer: 5'-GGA***AGATCT***GGAGCTATGGTGGTG-3', reverse primer: 5'-CGG***GGTACC***TTAGACACTAATCAGCTGGGG-3'). The PCR products of both XBP1u and

XBP1s were digested with *BglII and KpnI* and inserted to *pEGFP-C1* (Clontech). The forward primer 5'- GGA***AGATCT***GGAGCTATGGTGGTG-3' and reverse primer 5'-CGG***GGTACC***TTATACCGCCAGAATCCATGGGGAGATG-3' were used to amplify the coding sequence of the dominant negative form of XBP1, which was inserted between *BamHI* and *KpnI* in the vector pXJ40-FLAG. The expression plasmid for constitutively active Akt pcDNA-myr-AKT1 was a generous gift from Dr. Jean-Ehrland Ricci as described before (27).

Transfection of plasmids DNA to H1299 cells was performed using Lipofectamine 2000 reagent (Invitrogen) according to the manufacturer's instructions. Briefly, H1299 cells were plated to 12-well plate the day before transfection. For each well, 0.8 μg plasmid DNA and 2 μl Lipofectamine 2000 were each diluted with 100 μl RPMI and incubated for 5 minutes. Then the diluted plasmid and transfection reagent were mixed by brief vortex and incubated for another 20 minutes. The H1299 cells were changed with 800 μl RPMI containing 5% FBS and the transfection mixture was added to each well dropwise. The cells were incubated at 37^{o}C for 6-8 hours before replacing with complete medium. At 24 hours post-transfection, cells were infected with IBV at an MOI of 2 or mock infected and continued incubated before harvested for protein and/or RNA analysis at indicated time points.

RNA interference

IRE1α siRNA (+): 5'-GGACGUGAGCGACAGAAUA dTdT-3', XBP1 siRNA (+): 5'-ACAGCAAGUGGUAGAUUUA dTdT-3', JNK1/2 siRNA (+): 5'-AAAGAAUGUCCUACCUUCU dTdT-3', and control EGFP siRNA (+): 5'-GCUGACCCUGAAGUUCAUC dTdT-3' were purchased from Sigma (28, 29). Transfection of siRNA was performed using DhamaFECT2 transfection reagent (Dharmacon, Thermo Fisher Scientific) according to the manufacturer's instructions. At 48 hours post-transfection, cells were infected with IBV at an MOI of 2 or mock infected and continued incubated before harvested for protein and/or RNA analysis at indicated time points.

RNA extraction and RT-PCR analysis

Total RNA from cultured cells was extracted with TRIzol Reagent (Invitrogen) according to the manufacturer's instructions. Briefly, cells were lysed with 1 ml TRIzol per 10 cm^2 effective growth area and the lysates were mixed with one-fifth volume of chloroform. After centrifugation at 12,000 g at 4^oC for 15 minutes, the aqueous phase was mixed with equal volume of isopropanol. RNA was pelleted by centrifugation at 12,000 g at 4^oC for 15 minutes, washed with 70% ethanol twice and dissolved in RNase-free H_2O. The concentration of the total RNA was measured using a NanoDrop 1000 Spectrophotometer (Thermo Fisher Scientific).

The cDNA was reverse transcribed from total RNA using oligo-dT and ImProm-II™ Reverse Transcription System (Promega) according to the manufacturer's instructions. The following primers (forward and reverse) were used for PCR: IRE1α: GAAAAGGAATCCCTGGATGG and TCAGAGGGCGTCTGGAGTC; XBP1: CAGCGCTTGGGGATGGATGC and GGGCTTGGTATATATGTGG; ERdj4: GATACACTTGGACACAGTGC and CTACTGTCCTGAACAGTCAG; EDEM1: CTACCAGGCAACCAAGAATC and CCAACCATCTGGTCAATCTG; P58IPK: GGCTCGGTATTCCCCTTCCT and AGTAGCCCTCCGATAATAAGCAA; HERPUD1: GGACCTATTCAGCAGCTACA and ATCAGTTTGCGATGGCTGGG; GAPDH: GGGCTCATCTGAAGGGTGGTGC and GGACGCTGGGATGATGTTCTGG; IBV gRNA, GAGTAACATAATGGACCTGT and TGCTGTACCCTCGATCGTAC; IBV sgRNA2, CTATTACACTAGCCTTGCGCTAGA and CTCTGGATCCAATAACCTAC. The PCR products were resolved using 1% agarose gel pre-stained with ethidium bromide and visalized under UV shadowing. The band intensities of specific genes were determined by densitometry using Image J software and normalized to the intensities of corresponding GAPDH bands. To resolve the unspliced and spliced form of XBP1, the PCR products were resolved using 4% agarose gel. Percentage of XBP1 splicing [XBP1s (%)] was calculated as the intensity of XBP1s divided by the total intensities of XBP1u and XBP1s.

Real time RT-PCR was performed using SYBR select PCR kit (Life technologies) in an Applied Biosystems 7500 real-time PCR system (Applied Biosystems) according to manufacturer's

instructions. The mRNA levels of specific genes were calculated using GAPDH as an internal reference and normalized to 0 hour samples (in time course experiments) or siEGFP transfected samples (in siRNA knockdown experiments). The following real time PCR primers (forward and reverse) were used: IRE1α: CGGGAGAACATCACTGTCCC and CCCGGTAGTGGTGCTTCTTA; Total XBP1: TTGTCACCCCTCCAGAACATC and TCCAGAATGCCCAACAGGAT; Spliced XBP1: TGCTGAGTCCGCAGCAGGTG and GCTGGCAGGCTCTGGGGAAG; ERdj4: TCTTAGGTGTGCCAAAATCGG and TGTCAGGGTGGTACTTCATGG; EDEM1: CGGACGAGTACGAGAAGCG and CGTAGCCAAAGACGAACATGC; P58IPK: GGCTCGGTATTCCCCTTCCT and AGTAGCCCTCCGATAATAAGCAA; GAPDH: CCACTCCTCCACCTTTGAC and ACCCTGTTGCTGTAGCCA.

SDS-PAGE and Western blot analysis.

Cells were infected with IBV and harvested at indicated times points using cell scrapers (Corning). After centrifugation at 16,000 g for 1 minute, the supernatant was discarded and the pellets were lysed in 1X RIPA buffer. After clarifying by centrifugation and determination of protein concentration by spectrophotometer, the cell lysates were mixed with Laemmli sample buffer containing 100 mM dithiothreitol (30). The protein samples were boiled at 90^{o}C for 5 minutes and centrifuged at 16,000 g for 5 minutes. Equal amount of protein samples were subjected to sodium dodecyl sulfate-polyacrylamide gel electrophoresis (SDS-PAGE) and transferred to 0.2 µm nitrocellulose membranes (Bio-Rad). After the nonspecific antibody binding sites were blocked with 5% skim milk in Tris-buffered saline (20 mM Tris-HCl pH 7.4, 150 mM NaCl) containing 0.1% Tween 20, the membranes were incubated with 1 µg/ml primary antibodies at 4 ^{o}C overnight. After washing with Tris-buffered saline, the membranes were incubated with 1:2000 diluted anti-mouse or anti-rabbit IgG antibodies conjugated with horseradish peroxidase (DAKO) at room temperature for 2 hours. The membranes were washed and the proteins detected with a chemiluminescence detection kit (Amersham Biosciences) and medical X-ray films (Fujifilm) according to the manufacturer's

instructions. The films were scanned as gray scale 8-bit images and the density of bands were determined by the NIH software ImageJ.

Virus titration

Cell-free supernatants of IBV infected cells collected at different time points were clarified by centrifugation and 10-fold serially diluted using serum-free DMEM. The viral titers were determined by plaque assay. Briefly, 250 µl diluted supernatants were applied to confluent monolayers of Vero cells in 6-well plates. The plate was agitated every 10 minutes to ensure proper coverage of the monolayers. After 2 hours of adsorption, unbound viruses were removed and cells were washed twice with DMEM. 2 ml overlay medium (0.4% agarose in DMEM) was added to each well and the plates were incubated at 37^{o}C for two days before plaques formed. Agarose overlay was removed and cells fixed with 4% formaldehyde before staining with crystal violet. Finally plaque numbers were count and the titers of individual samples were expressed in the unit of logarithm of plaque forming unites (PFU) per ml. Each sample was titrated in triplicate in each experiment.

Results

IBV infection activates the IRE1α-XBP1 pathway

Our previous studies have shown that the PERK branch of the ER stress response is activated in cells infected with IBV at early stage of infection (31, 32). To determine whether IBV infection also modulates the IRE1α pathway, H1299 cells were either infected with IBV at a multiplicity of infection (MOI) ~ 2 or incubated with UV-inactivated IBV (UV-IBV). Cells treated with DTT, a strong ER stress inducer, were included as a positive control. Total RNAs were extracted and subjected to semi-quantitative RT-PCR analysis. The IBV genomic RNA could be detected from 12 hours post-infection (hpi) and accumulated till the end of infection (Figure 1a). RT-PCR analysis of HERPUD1, a component of the ERAD pathway and a commonly used ER stress marker (33, 34), showed significant increase at the mRNA level in cells infected with IBV and treated with DTT, but not in cells incubated with UV-IBV (Figure 1a). Therefore, similar to other coronaviruses studied, IBV infection induces potent ER stress. Determination of the mRNA levels of components in the IRE1α-XBP1 pathway of the UPR showed stable increase of IRE1α through the course of infection with slight reduction at 24 hpi, possibly due to extensive cell death at late stage of infection (Figure 1a). The total amount of XBP1 mRNA was also gradually accumulated over time, whereas both IRE1α and XBP1 mRNA remained relatively unchanged in cells incubated with UV-IBV (Figure 1a).

During ER stress, the activated IRE1α mediates splicing of the XBP1 mRNA by removing a 26-nt intron, as previously described (6). A moderate degree of XBP1 splicing (~15%) was detected in IBV-infected H1299 cells at 24 hpi, as compared to ~90% splicing in cells treated with DTT (Figure 1a). No XBP1 splicing was observed in cells incubated with UV-IBV (Figure 1a). ERdj4, EDEM1 and P58IPK are known to be specifically induced by the spliced form of XBP1 (9). A significant induction of all three genes were observed in cells treated with DTT. Considerable increase of ERdj4 mRNA was detected in IBV infected cells, but only moderate induction of P58IPK and EDEM1 by IBV infection was observed (Figure 1a). Since ERdj4 has been shown to be specifically induced by XBP1s, it was interesting to note that ERdj4 was induced in the IBV-infected

cells in the absence of detectable spliced XBP1 at early time points (8-20h). The same time course experiment was performed in Vero cells. Similarly, the mRNA levels of HERPUD1, IRE1α, XBP1, EDEM1, P58IPK and ERdj4 were up-regulated in IBV-infected Vero cells, and a moderate level of XBP1 splicing was observed at 24 hpi (Figure 1a, right panels).

To confirm the semi-quantitative RT-PCR results, real time-RT-PCR was performed. As shown in Figure 1b, IBV infection induced a ~12-fold increase in IRE1α mRNA and a ~4-fold increase in total XBP1 mRNA in H1299 cells at 20 hpi. The mRNA level of XBP1s was determined using a pair of primers previously validated to amplify only the spliced variant (35). Compared with mock infected control, IBV infection induced a ~18-fold increase in XBP1s mRNA. Consistantly, ERdj4, EDEM1 and P58IPK mRNA level increased by ~2-3 fold in IBV infected cells as compared with the mock infected control (Figure 1b). The same pattern was also observed in Vero cells, where IBV infection induced significant up-regulation of IRE1α, total XBP1, XBP1s, ERdj4 and P58IPK (Figure 1b, lower panels). Taken together, IBV infection causes ER stress in the infected cells and activates the IRE1α-XBP1 pathway.

Knockdown of IRE1α and XBP1 attenuates IBV-induced activation of the IRE1α-XBP1 pathway

To confirm that the IRE1α-XBP1 pathway is induced in IBV-infected cells, we used siRNA to specifically knock down IRE1α or XBP1 in H1299 cells. Vero cells were not chosen for the knockdown experiments due to its very low transfection efficiency. As shown in Figure 2a, H1299 cells were transfected with siRNAs targeting IRE1α, XBP1 or EGFP (as negative control) before treated with DTT. As expected, the mRNA level of IRE1α, total XBP1, XBP1s and ERdj4 significantly increased in the siEGFP transfected DTT-treated cells, compared with mock-treated control. Transfection of siIRE1α significantly reduced DTT-induced up-regulation of IRE1α and XBP1 splicing by ~50%. On the other hand, transfection of siXBP1 drastically reduced the mRNA level of total XBP1 and spliced XBP1 induced by DTT by ~70%. Moreover, knockdown of either IRE1α or XBP1 also reduced DTT-induced ERdj4 up-regulation by 30-40%. These suggested that

transfection of the siRNAs specifically reduced the mRNA level of target genes and down-regulated the activation of IRE1α-XBP1 pathway triggered by DTT.

We then infected the siRNA-transfected cells with IBV, harvest total RNA at 20 hpi and compared the mRNA level of genes related to the IRE1α-XBP1 pathway using RT-qPCR. As shown in Figure 2b, transfection with siIRE1α and siXBP1 resulted in ~75% and ~90% knockdown efficiencies in the endogenous IRE1α and total XBP1 mRNA level, respectively. Compared with the DTT treatment experiment, the higher knockdown efficiency could be a result of longer incubation time after siRNA transfection before cell harvest. Notably, whereas siXBP1 nearly completely abolished the IBV-induced up-regulation of XBP1s, siIRE1α also reduced the level of XBP1s mRNA by ~75% (Figure 2b). This is not surprising, because IRE1α is required for efficient splicing of XBP1 in cells under ER stress. Knockdown of IRE1α or XBP1 significantly reduced IBV-induced up-regulation of ERdj4 and P58IPK by more than 50%, but the mRNA level of EDEM1 was only minimally affected (Figure 2b). Therefore, IBV infection indeed activates the IRE1α-XBP1 pathway, and the IBV-induced up-regulations of downstream genes ERdj4 and P58IPK were dependent on both IRE1α and XBP1.

Knockdown of IRE1α potentiates IBV-induced apoptosis in infected cells

One outcome of cells under ER stress is the activation of caspase-dependent apoptosis and IRE1α has been previously demonstrated to mediate ER stress-induced apoptosis (12-14). We next looked at the role of IRE1α and XBP1 in IBV-induced apoptosis. As shown in Figure 3a, H1299 cells were transfected with siIRE1α, siXBP1 and siEGFP, before infected with IBV or mock infected. The knockdown efficiencies were determined by Western blot, although we were only able to detect the unspliced form but not the spliced form of XBP1. Successful knockdown of the two genes were also reflected by the effects on XBP1 splicing determined by RT-PCR. Consistent with the real time PCR results (Figure 2b), whereas knockdown of IRE1α reduced the mRNA level of spliced XBP1, knockdown of XBP1 depleted the mRNA of both XBP1u and XBP1s. Poly (ADP-ribose) polymerase (PARP), a well characterized apoptosis marker and a cleavage target of caspase 3, was

used to monitor apoptosis. In cells transfected with siEGFP, significant PARP cleavage (~27%) was detected at 22 hpi. Interestingly, in IRE1α-knockdown cells, PARP cleavage could be detected at an earlier time point (~19 hpi). Moreover, at 22 hpi, a more prominent PARP cleavage (~49%) was ovserved in IBV-infected IRE1α-knockdown cells, compared with the siEGFP control (Figure 3a). Surprisingly, knockdown of XBP1 did not result in a similar phenotype. Indeed, in XBP1-knockdown cells, no significant PARP cleavage could be detected throughout the course of infection (Figure 3a). The same experiment was performed multiple times, and the observed effects of gene knockdown on IBV-induced PARP cleavage were reproducible and statistically significant (Figure 3b).

To further validate the results, we also determined the activation of caspases (Caspase 3, 8 and 9) during IBV infection in the knockdown cells. Samples collected at 22 hpi and siEGFP trasnfected mock infected sample in Figure 3a were further probed with individual caspase antibodies. As shown in Figure 3c, consistent with the PARP cleavage pattern, the percentages cleavage of caspase 3, 8 and 9 were significantly higher in IRE1α-knockdown cells, and lower in XBP1-knockdown cells, as compared with the siEGFP control. The knockdown of IRE1α or XBP1 did not affect IBV replication, as determinded by the similar N protein level (Figure 3a) and the similar virus titers in the supernatant (Figure 3d). Taken together, these data suggest that although IRE1α is not essential for IBV replication, it protects the infected cells from IBV-induced apoptosis.

The seemingly opposite effect of XBP1 knockdown on apoptosis was unexpected, since XBP1 is the main target of IRE1α mediated splicing. However, it is well known that whereas XBP1s serves as a potent activator of downstream UPR genes, XBP1u is actually a negative regulator of UPR (36). Therefore it is possible that XBP1u and XBP1s may also demonstrate opposite effects on IBV-induced apoptosis. Because siXBP1 used in the experiments targets both XBP1u and XBP1s, it is difficult to elucidate the function of individual isoforms. As shown in the later section, when we shifted to the over-expression approach using wild type and dominant negative XBP1, it became appearent that XBP1u and XBP1s indeed exert opposite effect on IBV-induced apoptosis.

353 **Overexpression of full-length IRE1α protects cells from IBV-induced apoptosis**

354 We next adopted the transient overexpression approach to study the anti-apoptotic activity of IRE1α.
355 A plasmid encoding the full-length human IRE1α with an HA-tag at the C-terminus was constructed.
356 H1299 cells were transfected with the construct or vector control (pcDNA3.1), before infected with
357 IBV at an MOI ~2 or mock infected. As shown in Figure 4a, the expression of IRE1α-HA was
358 detected by western blot using antibodies against the HA-tag. Transfection of IRE1α did not
359 significantly affect the replication of IBV, as indicated by the similar level of N protein compared
360 with the control (Figure 4a). In the vector control, IBV induced prominent PARP cleavage at 20 hpi
361 (~20%) and 24 hpi (~46%). However, in cells transfected with IRE1α-HA, IBV-induced PARP
362 cleavage was partially reduced to ~9% at 20 hpi and ~24% at 24 hpi. The experiment was performed
363 multiple times and the reduction of PARP cleavage by transfection of full-length IRE1α was
364 reproducible and statistically significant (Figure 4b). Thus, ectopic expression of IRE1α could indeed
365 protect cells from IBV-induced apoptosis.

366 The IRE1α protein contains a lumenal domain that recognizes unfolded protein, a kinase
367 domain that triggers autophosphorylation and dimerization, and an RNase domain that mediates
368 XBP1 mRNA splicing (Figure 4c). To determine which domain of IRE1α is required for its anti-
369 apoptotic activity, a kinase dead mutant (K599A) and an RNase deletion mutant (ΔRNase) were
370 generated (Figure 4c). H1299 cells were transfected with vector, wild type IRE1α, or the two
371 mutants before infected with IBV or mock infected for 24 hours. As shown in Figure 4d, the
372 expression of transfected plasmids was determined by western blot. The protein level of wild type
373 IRE1α was lower than the two mutants, possibly because removal of the kinase or RNase activity
374 reduced the basal activation and subsequent degradation of the protein, rendering it more stable.
375 Transfection of wild type IRE1α, but not the kinase dead or RNase deletion mutants, significantly
376 increased the IBV-induced XBP1 splicing and up-regulation of ERdj4, compared with the vector
377 control (Figure 4d). As expected, over-expression of wild type IRE1α partially reduced IBV-induced
378 PARP cleavage. However, in IBV-infected cells transfected with the IRE1α mutants, PARP cleavage

was indeed slightly higher compared with the vector control (Figure 4d). IBV replication is not significantly affected by transfection of the constructs, as indicated by similar IBV N level. Therefore, the result suggested that both the kinase and RNase activities of IRE1α are required for its anti-apoptotic activity during IBV infection.

Overexpression of XBP1s, but not XBP1u, protects cells from IBV-induced apoptosis

Because siRNA for XBP1 targets both the unspliced and the spliced form, it is difficult to attribute the observed phenotype to individual isoforms. Therefore we have also adopted the overexpression approach to study the function of XBP1u and XBP1s during IBV infection. Initially, the coding sequence of XBP1u or XBP1s was inserted into the C-terminal HA-tagged pcDNA3.1 vector as used for IRE1α constructs above. However, when transfected into H1299 cells, the protein expression level was very low for both XBP1u-HA and XBP1s-HA (data not shown). To enhance the expression level and monitor transfection efficiency, XBP1u and XBP1s were fused with N-terminal EGFP-tag (37). As shown in Figure 5a, H1299 cells were transfected with EGFP-XBP1u, EGFP-XBP1s or vector plasmid, before infected with IBV or mock infected. Using anti-EGFP antibody, the expression of both fusion proteins were clearly detectable. Many degradation bands could be detected for XBP1u, which is probably due to the proteosome degradation motif in the C-terminal region as described previously (36). Transfection of EGFP-XBP1u or EGFP-XBP1s did not significantly affect the replication of IBV, as determined by the similar level of IBV N protein compared with the control (Figure 5a). It was noted that the levels of IBV+gRNA at 24 hpi in the EGFP-XBP1u or EGFP-XBP1s transfected cells seemed to be lower than that of the control. But the intensity ratios were actually very similar after normalized to the GAPDH bands. Detection of similar amounts of IBV+gRNA in all transfected cells at the same timepoint was also confirmed by real time PCR analysis. Therefore, IBV replication was not affected by the over-expression of EGFP-XBP1u or EGFP-XBP1s. As shown in Figure 5a, transfection of EGFP-XBP1s but not EGFP-XBP1u significantly enhanced the IBV-induced up-regulation of ERdj4, indicating that the ectopic

405 expressed XBP1s had normal function as a potent UPR transcription factor. Compared with the
406 vector control, in cells transfected with EGFP-XBP1u, a weak level of PARP cleavage could be
407 detected at an early time point (20 hpi), and a slightly higher PARP cleavage was also observed at 24
408 hpi. These suggested that XBP1u might function as a weak pro-apoptotic protein during IBV
409 infection. In contrast, in cells transfected with EGFP-XBP1s, the IBV-induced PARP cleavage was
410 lower than in the control at 24 hpi. Although the difference is not intense, it is observed in multiple
411 experiments and statistically significant (Figure 5b). Therefore, unlike XBP1u, the XBP1s protein
412 demonstrated anti-apoptotic characteristic during IBV infection.

413 Both XBP1u and XBP1s contain the bZIP DNA binding domain in the N-terminal (Figure
414 5c). In XBP1u, the presence of a proteasome degradation motif renders it highly unstable in the cells.
415 On the other hand, due to the frameshifting resulted from IRE1α-mediated splicing, XBP1s encodes
416 a transactivation domain at the C-terminal that accounts for its ability to induce downstream UPR
417 genes. Previous studies have established that when the proteasome degradation motif of XBP1u is
418 deleted, the resulted protein is stablized and served as a dominant negative inhibitor of XBP1s (38)
419 (Figure 5c). Therefore we decided to investigate the effect of this dominant negative XBP1 (XBP1-
420 DN) on IBV-induced apoptosis. As shown in Figure 5d, the expression of FLAG-tag XBP1-DN was
421 clearly detected. Multiple bands were observed possibly due to post-translational modifications of
422 the protein. Compared with the vector control, overexpression of XBP1-DN significantly enhanced
423 IBV-induced PARP cleavage, especially at the late time point 22 hpi. The pro-apoptotic effect of
424 XBP1-DN was also reflected by the much stronger cleavage of the IBV N protein, because
425 coronavirus N protein has been shown to be a substrate of activated caspases (39, 40). The
426 observation was reproducible and statistically significant (Figure 5e), suggesting that inhibition of
427 XBP1s by over-expressing XBP1-DN markedly potentitates IBV-induced apoptosis. Taken together,
428 the two isoforms of XBP1 display distinct properties during IBV infection: XBP1u is a weak pro-
429 apoptotic protein, whereas XBPs is an anti-apoptotic protein.

The kinases JNK and Akt are involved in the anti-apoptotic function of IRE1α

Since the MAP kinase JNK has been implicated in ER-stress induced apoptosis mediated by IRE1α (12), we moved on to investigate the involvement of JNK in IBV-induced apoptosis in H1299 cells. As shown in Figure 6a, a time course IBV infection experiment was performed in H1299 cells. As previously described, cells with IRE1α knocked down had an earlier onset and a significantly higher level of PARP cleavage compared with negative control samples of the same time point. Interestingly, we also observed significant differences in the phosphorylation level of two kinases: the pro-apoptotic kinase JNK and the pro-survival kinase Akt. In the negative control, relatively weak JNK phosphorylation was detected at 16 and 20 hpi. In contrast, in IRE1α-knockdown cells, JNK phosphorylation could be detected earlier (12 hpi) and to a significantly higher level compared with the control samples of the same time point (Figure 6a). On the other hand, phosphorylation of Akt was significantly induced at 8 hpi and sustained to 20 hpi in the negative control cells infected with IBV. However, in IRE1α-knockdown cells, significant Akt phosphorylation could be observed only at 12 hpi and rapidly diminished at 16 hpi (Figure 6a). Therefore, the hypo-phosphorylation of Akt and the hyper-phosphorylation of JNK may contribute to the enhanced IBV-induced apoptosis observed in the IRE1α-knockdown cells.

Next we perform further experiments to confirm the involvement of Akt and JNK in IBV-induced apoptosis. As shown in Figure 6b, H1299 cells were transfected with a constitutive active form of Akt (myr-AKT1) (27) or the vector control before infected with IBV. The expression of the transfected Akt could be determined by the significantly higher level of total Akt protein as well as the highly intense phosphor-Akt bands in the transfected samples. Transfection of constitutively active Akt did not affect IBV replication, indicated from the similar level of IBV N protein. In the vector control, IBV induced PARP cleavage at 20 and 22 hpi (Figure 6b). In contrast, PARP cleavage is completely abolished in cells transfected with myr-AKT1. Therefore, Akt is indeed a very strong anti-apoptotic protein during IBV infection.

In another experiment, H1299 cells were transfected with siRNA targeting JNK1/2 or EGFP, before infected with IBV or mock infected (Figure 6c). The knockdown of JNK was determined by the lower levels of both phosphor-JNK and total JNK in the siJNK1/2 transfected cells. JNK knockdown did not significantly affect IBV replication as indicated from the similar level of IBV N protein. In cells transfected with siJNK1/2, IBV-induced PARP cleavage was significantly reduced compared with the negative samples of the same time points (Figure 6c). Thus, it is quite likely that JNK plays a pro-apoptotic role during IBV infection.

Discussion

Being the primary site of protein synthesis and folding, the ER is a front line in the battle between virus and host cell. The infection of many RNA viruses is known to induce modification of the ER membrane and cause ER stress (17, 28, 37, 41). The replication and maturation of coronavirus are intimately associated with the ER, and ER stress is induced possibly through multiple mechanisms (42). First, massive synthesis of the highly glycosylated spike protein incurs significant burden to the ER (33, 43). Secondly, rearrangement of ER membrane structure for the formation of double membrane vesicles (16). Thirdly, extensive use of membrane from ER-Golgi intermediate compartment (ERGIC) for virus morphogenesis and budding. Moreover, the envelope proteins of SARS-CoV and other coronaviruses have been demonstrated to have membrane permeabilization and ion channel activities (44-46). The envelope protein of SARS-CoV has also been demonstrated to suppress the IRE1-XBP1 pathway of the UPR and inhibit virus-induced apoptotic cell death. In this study, we found that IBV infection induced ER stress and activated the IRE1α-XBP1 pathway of UPR, as indicated by the up-regulation of HERPUD1, IRE1α, total XBP1, XBP1s, ERdj4 and P58IPK mRNA in IBV-infected cells. IBV infection also increased the mRNA and protein levels of GRP78 and GRP94 (data not shown), two protein chaperones commonly used as markers of ER stress. Together with the recent publications on MHV and SARS-CoV, these findings demonstrate

479 that induction of ER stress and the UPR is a general host response during infection with
480 coronaviruses (17, 33).

481 In the previous study on MHV, up to 75% XBP1 splicing was observed in MHV-infected
482 cells, although the protein level of XBP1s was found to be only slightly increased (17). Similarly,
483 significant XBP1 splicing was detected in IBV-infected cells at late stage of infection. Although we
484 were not able to detect a specific band of XBP1s using western blot, a significant induction of
485 downstream UPR genes, such as ERdj4 and $P58^{IPK}$, was observed in IBV-infected cells. Moreover,
486 when the endogenous level of IRE1α or XBP1was depleted by siRNA, the mRNA level of ERdj4
487 and $P58^{IPK}$ was significantly reduced compared with the control. Also, when IRE1α or XBP1s was
488 overexpressed in the cells, the mRNA level of ERdj4 was markedly increased. These results
489 suggested that IBV infection indeed activated the IRE1α-XBP1 pathway, and the induction of UPR
490 genes required both IRE1α-mediated XBP1 splicing and the action of the XBP1s protein. On the
491 other hand, it is important to note that coronavirus may employ various strategies to suppress UPR
492 activation. For example, the E protein of SARS-CoV has been shown to inhibit XBP1 splicing and
493 suppress ER stress induced by infection with SARS-CoV and respiratory syncytial virus (18).
494 Whereas in MHV-infected cells, sustained translation shutdown via the eIF2α phosphorylation has
495 been attributed to the low level of XBP1s synthesis and the failure to induce UPR downstream genes
496 (17). Whether similar mechanisms apply to IBV infection remain to be investigated in the future.

497 Apoptosis is one possible outcome of cells infected with coronaviruses. Programmed
498 demolition of the infected cells can eliminate viruses before infectious progenies are formed.
499 However, if occurred at a later stage, apoptosis can also facilitate virus spread. When neighboring
500 cells engulf apoptotic bodies containing infectious virions, the viruses gain access to new host cells
501 without an extracellular stage and subvert recognition by the immune system. Previous studies have
502 demonstrated that coronaviruses induce caspase-dependent and p53-independent apoptosis in the
503 infected cells (19, 20, 47). In this study we investigated the involvement of the IRE1α-XBP1
504 pathway of UPR in IBV-induced apoptosis. The anti-apoptotic activity of IRE1α was clearly

505 demonstrated by the potentiated cleavage of PARP and caspases in IRE1α-knockdown cells infected
506 with IBV, and the partially reduced apoptosis when cells were overexpressing wild type IRE1α but
507 not its mutants. To our surprise, contrary to IRE1α, knockdown of XBP1 seemed to inhibit IBV-
508 induced apoptosis. However, since siXBP1 targeted both XBP1u and XBP1s, the contribution of
509 individual isoforms could not be determined. Further experiments using the overexpression approach
510 demonstrated that whereas unspliced XBP1 was pro-apoptotic, the spliced form is anti-apoptotic.
511 This is further confirmed when a stabilized, dominant negative form of XBP1 was transfected, IBV-
512 induced apoptosis was significantly potentiated. Considering the fact that IBV induced relatively low
513 level of XBP1 splicing compared to DTT treatment and that only XBP1u but not XBP1s could be
514 detected using western blot, it is likely that the pre-dominant isoform of XBP1 in the infected cells
515 was the unspliced form. This may explain why a lower level of IBV-induced apoptosis was observed
516 when XBP1 was knocked down using siRNA. In that case, the anti-apoptotic function of IRE1α may
517 be mediated, at least in part, via the conversion of pro-apoptotic XBP1u to anti-apoptotic XBP1s.
518 Previous studies have shown that under prolong ER stress, the MAP kinase JNK is
519 phosphorylated by IRE1α to induce apoptosis (12). Activation of JNK could be detected in cells
520 infected with SARS-CoV (48), MHV-A59 (49) or IBV. If JNK phosphorylation was mediated by
521 IRE1α in coronavirus-infected cells, a reduced level of phosphor-JNK would be detected in IRE1α-
522 deficient cells. However, the enhanced IBV-induced apoptosis observed in IRE1α-knockdown cells
523 was associated with a hyper-phosphorylation of JNK. In fact, knockdown of JNK partially reduced
524 IBV-induced PARP cleavage, suggesting that JNK was pro-apoptotic in nature. Therefore, it is likely
525 that during IBV infection, JNK was activated by other upstream kinases (such as MKK4/MKK7) to
526 promote apoptosis, which was modulated by the uncharacterized activity of IRE1α.
527 On the other hand, the Akt kinase has been demonstrated to play an important role in cell
528 survival under ER stress (50). Previous studies on SARS-CoV demonstrated that limited activation
529 of Akt was observed at early stage of infection, but could not prevent virus-induced apoptosis (51).
530 In the current report, we found that enhanced IBV-induced apoptosis in IRE1α-knockdown cells was

associated with hypo-phosphorylation of Akt. So far, there has been no report of direct phosphorylation of Akt by the kinase activity of IRE1α. Of note, it has been shown that inhibition of Akt phosphorylation actually promote the activity of IRE1α and IRE1α-mediated JNK phosphorylation (52). Therefore, the signaling between Akt and IRE1α seems to be complicated, which may differ in cells under various stress conditions and may involve the actions of other regulatory factors. The signaling cross-talks between Akt and JNK may also be complicated in nature. As a survival kinase, Akt has been known to decrease the kinase activity of ASK1, which is the upstream MAP kinase kinase kinase of JNK (53). Moreover, Akt also interacts with JNK interacting protein-1 (JIP1) and prevent its association with JNK to form active signaling comples (54). On the other hand, it has been shown that JNK can inhibit the survival signals of Akt by phosphorylating the 14-3-3 protein (55). It is possible that the phosphorylation status and antagonizing actions of Akt and JNK serve important function in determining the cell death/survival at the late stage of IBV infection, and as an ER stress sensor, IRE1α modulates the phosphorylation of Akt and JNK to promote cell survival.

To summarize the findings in the current study, we proposed a working model in Figure 7. IBV infection induces ER stress and the activation of IRE1α. IRE1α mediates splicing of XBP1 and downstream UPR genes (such as ERdj4 and $p58^{IPK}$) are up-regulated to restore ER homeostasis. Whereas the unspliced form of XBP1 is pro-apoptotic, the spliced form is anti-apoptotic. IRE1α protect cells from IBV-induced apoptosis, possibly by mediating the splicing of XBP1 and converting it from the pro-apoptotic XBP1u to anti-apoptotic XBP1s. IRE1α also modulate the phosphorylation status of the kinase Akt and JNK during IBV infection. The activation of the pro-survival kinase Akt seems to be promoted by IRE1α, whereas the phosphorylation of the pro-apoptotic kinase JNK seems to be negatively regulated by IRE1α (Figure 7).

Previously, we have demonstrated that the PERK branch of UPR and the dsRNA dependent kinase PKR are activated at the early stage of IBV infection (31). These lead to phosphorylation of eIF2α and up-regulation of the growth arrest and DNA damage inducible protein 153 (GADD153),

557 which promotes IBV-induced apoptosis by suppressing the pro-survival extracellular signal related
558 kinase (ERK) (31). Among the three UPR sensors, PERK is generally believed to be activated first in
559 response to ER stress, followed by ATF6 and IRE1α (1, 56). It is interesting to consider the temporal
560 control of UPR activation and its implication in coronavirus infection. From the host perspective,
561 early activation of the PERK pathway and eIF2α phosphorylation induces translation attenuation,
562 which serves as an effective anti-viral defense mechanism. The induction of apoptosis through the
563 eIF2α-ATF4-GADD153 pathway may also restrict virus replication. On the other hand, activation of
564 the IRE1α at the late stage of infection seems to promote survival of the infected cells. This may
565 allow more virions to be assembled and released before the infected cells succumb to apoptotic cell
566 death. Moreover, the cross-talks between UPR and innate immune response may also constitute an
567 important aspect of anti-viral response during coronavirus infection (42).
568 In conclusion, the current study demonstrates that IRE1α, a major ER stress transducer,
569 modulate apoptosis signaling during coronavirus infection. This work reveals the anti-apoptotic
570 signaling of UPR in cells infected with IBV and provides new insights into the intricate signaling
571 networks in the IBV-induced apoptosis.
572

Acknowledgement

This work was partially supported by a Competitive Research Programme (CRP) grant (R-154-000-529-281), the National Research Foundation, Singapore, and an Academic Research Fund (AcRF) Tier 1 grant (RGT17/13), Nanyang Technological University and Ministry of Education, Singapore.

References

1. **Ron D, Walter P.** 2007. Signal integration in the endoplasmic reticulum unfolded protein response. Nat Rev Mol Cell Biol **8:**519-529.
2. **Shi Y, Vattem KM, Sood R, An J, Liang J, Stramm L, Wek RC.** 1998. Identification and characterization of pancreatic eukaryotic initiation factor 2 α-subunit kinase, PEK, involved in translational control. Mol Cell Biol **18:**7499-7509.
3. **Ye J, Rawson RB, Komuro R, Chen X, Davé UP, Prywes R, Brown MS, Goldstein JL.** 2000. ER stress induces cleavage of membrane-bound ATF6 by the same proteases that process SREBPs. Mol Cell **6:**1355-1364.
4. **Wang Y, Shen J, Arenzana N, Tirasophon W, Kaufman RJ, Prywes R.** 2000. Activation of ATF6 and an ATF6 DNA binding site by the endoplasmic reticulum stress response. Journal of Biological Chemistry **275:**27013-27020.
5. **Bertolotti A, Zhang Y, Hendershot LM, Harding HP, Ron D.** 2000. Dynamic interaction of BiP and ER stress transducers in the unfolded-protein response. Nat Cell Biol **2:**326-332.
6. **Calfon M, Zeng H, Urano F, Till JH, Hubbard SR, Harding HP, Clark SG, Ron D.** 2002. IRE1 couples endoplasmic reticulum load to secretory capacity by processing the XBP-1 mRNA. Nature **415:**92-96.
7. **Yoshida H, Matsui T, Yamamoto A, Okada T, Mori K.** 2001. XBP1 mRNA is induced by ATF6 and spliced by IRE1 in response to ER stress to produce a highly active transcription factor. Cell **107:**881-891.
8. **Ng DT, Spear ED, Walter P.** 2000. The unfolded protein response regulates multiple aspects of secretory and membrane protein biogenesis and endoplasmic reticulum quality control. J Cell Biol **150:**77-88.
9. **Lee AH, Iwakoshi NN, Glimcher LH.** 2003. XBP-1 regulates a subset of endoplasmic reticulum resident chaperone genes in the unfolded protein response. Mol Cell Biol **23:**7448-7459.
10. **Taylor RC, Cullen SP, Martin SJ.** 2008. Apoptosis: controlled demolition at the cellular level. Nat Rev Mol Cell Biol **9:**231-241.
11. **Oyadomari S, Mori M.** 2003. Roles of CHOP/GADD153 in endoplasmic reticulum stress. Cell Death & Differentiation **11:**381-389.
12. **Urano F, Wang X, Bertolotti A, Zhang Y, Chung P, Harding HP, Ron D.** 2000. Coupling of stress in the ER to activation of JNK protein kinases by transmembrane protein kinase IRE1. Science **287:**664-666.
13. **Yoneda T, Imaizumi K, Oono K, Yui D, Gomi F, Katayama T, Tohyama M.** 2001. Activation of caspase-12, an endoplastic reticulum (ER) resident caspase, through tumor necrosis factor receptor-associated factor 2-dependent mechanism in response to the ER stress. J Biol Chem **276:**13935-13940.
14. **Hitomi J, Katayama T, Taniguchi M, Honda A, Imaizumi K, Tohyama M.** 2004. Apoptosis induced by endoplasmic reticulum stress depends on activation of caspase-3 via caspase-12. Neurosci Lett **357:**127-130.
15. **Snijder EJ, Van Der Meer Y, Zevenhoven-Dobbe J, Onderwater JJM, Van Der Meulen J, Koerten HK, Mommaas AM.** 2006. Ultrastructure and origin of membrane vesicles associated with the severe acute respiratory syndrome coronavirus replication complex. J Virol **80:**5927-5940.
16. **Knoops K, Kikkert M, Van Den Worm SHE, Zevenhoven-Dobbe JC, Van Der Meer Y, Koster AJ, Mommaas AM, Snijder EJ.** 2008. SARS-coronavirus replication is supported by a reticulovesicular network of modified endoplasmic reticulum. PLoS biology **6:**e226.
17. **Bechill J, Chen Z, Brewer JW, Baker SC.** 2008. Coronavirus infection modulates the unfolded protein response and mediates sustained translational repression. J Virol **82:**4492-4501.
18. **DeDiego ML, Nieto-Torres JL, Jiménez-Guardeño JM, Regla-Nava JA, Álvarez E, Oliveros JC, Zhao J, Fett C, Perlman S, Enjuanes L.** 2011. Severe Acute Respiratory Syndrome Coronavirus Envelope Protein Regulates Cell Stress Response and Apoptosis. PLoS Pathog **7:**e1002315.
19. **Liu C, Xu HY, Liu DX.** 2001. Induction of caspase-dependent apoptosis in cultured cells by the avian coronavirus infectious bronchitis virus. J Virol **75:**6402-6409.
20. **Li FQ, Tam JP, Liu DX.** 2007. Cell cycle arrest and apoptosis induced by the coronavirus infectious bronchitis virus in the absence of p53. Virology **365:**435-445.

21. **Zhong Y, Liao Y, Fang S, Tam JP, Liu DX.** 2012. Up-regulation of mcl-1 and bak by coronavirus infection of human, avian and animal cells modulates apoptosis and viral replication. PLoS One **7:**e30191.
22. **Zhong Y, Tan YW, Liu DX.** 2012. Recent Progress in Studies of Arterivirus-and Coronavirus-Host Interactions. Viruses **4:**980-1010.
23. **Ng LF, Liu DX.** 1998. Identification of a 24-kDa polypeptide processed from the coronavirus infectious bronchitis virus 1a polyprotein by the 3C-like proteinase and determination of its cleavage sites. Virology **243:**388-395.
24. **Xu LH, Huang M, Fang SG, Liu DX.** 2011. Coronavirus Infection Induces DNA Replication Stress Partly through Interaction of Its Nonstructural Protein 13 with the p125 Subunit of DNA Polymerase δ. Journal of Biological Chemistry **286:**39546-39559.
25. **Liu DX, Inglis SC.** 1991. Association of the infectious bronchitis virus 3c protein with the virion envelope. Virology **185:**911-917.
26. **Li FQ, Xiao H, Tam JP, Liu DX.** 2005. Sumoylation of the nucleocapsid protein of severe acute respiratory syndrome coronavirus. FEBS Lett **579:**2387-2396.
27. **Jacquin M, Chiche J, Zunino B, Bénéteau M, Meynet O, Pradelli L, Marchetti S, Cornille A, Carles M, Ricci J.** 2013. GAPDH binds to active Akt, leading to Bcl-xL increase and escape from caspase-independent cell death. Cell Death & Differentiation **20:**1043-1054.
28. **Huang ZM, Tan T, Yoshida H, Mori K, Ma Y, Yen TS.** 2005. Activation of hepatitis B virus S promoter by a cell type-restricted IRE1-dependent pathway induced by endoplasmic reticulum stress. Mol Cell Biol **25:**7522-7533.
29. **Blanchard E, Belouzard S, Goueslain L, Wakita T, Dubuisson J, Wychowski C, Rouille Y.** 2006. Hepatitis C virus entry depends on clathrin-mediated endocytosis. J Virol **80:**6964-6972.
30. **Laemmli UK.** 1970. Cleavage of structural proteins during the assembly of the head of bacteriophage T4. Nature **227:**680-685.
31. **Liao Y, Fung TS, Huang M, Fang SG, Zhong Y, Liu DX.** 2013. Upregulation of CHOP/GADD153 during coronavirus infectious bronchitis virus infection modulates apoptosis by restricting activation of the extracellular signal-regulated kinase pathway. J Virol **87:**8124-8134.
32. **Wang X, Liao Y, Yap PL, Png KJ, Tam JP, Liu DX.** 2009. Inhibition of protein kinase R activation and upregulation of GADD34 expression play a synergistic role in facilitating coronavirus replication by maintaining de novo protein synthesis in virus-infected cells. J Virol **83:**12462-12472.
33. **Versteeg GA, Van De Nes PS, Bredenbeek PJ, Spaan WJM.** 2007. The coronavirus spike protein induces endoplasmic reticulum stress and upregulation of intracellular chemokine mRNA concentrations. J Virol **81:**10981-10990.
34. **Meir O, Dvash E, Werman A, Rubinstein M.** 2010. C/EBP-β regulates endoplasmic reticulum stress–triggered cell death in mouse and human models. PLoS One **5:**e9516.
35. **HIROTA M, KITAGAKI M, ITAGAKI H, AIBA S.** 2006. Quantitative measurement of spliced XBP1 mRNA as an indicator of endoplasmic reticulum stress. The Journal of toxicological sciences **31:**149-156.
36. **Yoshida H, Oku M, Suzuki M, Mori K.** 2006. pXBP1 (U) encoded in XBP1 pre-mRNA negatively regulates unfolded protein response activator pXBP1 (S) in mammalian ER stress response. J Cell Biol **172:**565-575.
37. **Yu CY, Hsu YW, Liao CL, Lin YL.** 2006. Flavivirus infection activates the XBP1 pathway of the unfolded protein response to cope with endoplasmic reticulum stress. J Virol **80:**11868-11880.
38. **Tirosh B, Iwakoshi NN, Glimcher LH, Ploegh HL.** 2006. Rapid turnover of unspliced Xbp-1 as a factor that modulates the unfolded protein response. Journal of Biological Chemistry **281:**5852-5860.
39. **Eléouët JF, Slee EA, Saurini F, Castagné N, Poncet D, Garrido C, Solary E, Martin SJ.** 2000. The viral nucleocapsid protein of transmissible gastroenteritis coronavirus (TGEV) is cleaved by caspase-6 and-7 during TGEV-induced apoptosis. J Virol **74:**3975-3983.
40. **Diemer C, Schneider M, Seebach J, Quaas J, Frösner G, Schätzl HM, Gilch S.** 2008. Cell type-specific cleavage of nucleocapsid protein by effector caspases during SARS coronavirus infection. Journal of molecular biology **376:**23-34.
41. **Pena J, Harris E.** 2011. Dengue virus modulates the unfolded protein response in a time-dependent manner. J Biol Chem **286:**14226-14236.

42. **Fung TS, Liu DX.** 2014. Coronavirus infection, ER stress, apoptosis and innate immunity. Frontiers in Microbiology **5:**1-13.
43. **Chan CP, Siu KL, Chin KT, Yuen KY, Zheng B, Jin DY.** 2006. Modulation of the unfolded protein response by the severe acute respiratory syndrome coronavirus spike protein. J Virol **80:**9279-9287.
44. **Liao Y, Lescar J, Tam J, Liu D.** 2004. Expression of SARS-coronavirus envelope protein in< i> Escherichia coli</i> cells alters membrane permeability. Biochem Biophys Res Commun **325:**374-380.
45. **Liao Y, Yuan Q, Torres J, Tam J, Liu D.** 2006. Biochemical and functional characterization of the membrane association and membrane permeabilizing activity of the severe acute respiratory syndrome coronavirus envelope protein. Virology **349:**264-275.
46. **Verdiá-Báguena C, Nieto-Torres JL, Alcaraz A, DeDiego ML, Torres J, Aguilella VM, Enjuanes L.** 2012. Coronavirus E protein forms ion channels with functionally and structurally-involved membrane lipids. Virology **432:**485-494.
47. **Eleouet JF, Chilmonczyk S, Besnardeau L, Laude H.** 1998. Transmissible gastroenteritis coronavirus induces programmed cell death in infected cells through a caspase-dependent pathway. J Virol **72:**4918-4924.
48. **Mizutani T, Fukushi S, Saijo M, Kurane I, Morikawa S.** 2005. JNK and PI3k/Akt signaling pathways are required for establishing persistent SARS-CoV infection in Vero E6 cells. Biochimica et Biophysica Acta (BBA)-Molecular Basis of Disease **1741:**4-10.
49. **Yu D, Zhu H, Liu Y, Cao J, Zhang X.** 2009. Regulation of proinflammatory cytokine expression in primary mouse astrocytes by coronavirus infection. J Virol **83:**12204-12214.
50. **Hu P, Han Z, Couvillon AD, Exton JH.** 2004. Critical role of endogenous Akt/IAPs and MEK1/ERK pathways in counteracting endoplasmic reticulum stress-induced cell death. Journal of Biological Chemistry **279:**49420-49429.
51. **Mizutani T, Fukushi S, Saijo M, Kurane I, Morikawa S.** 2004. Importance of Akt signaling pathway for apoptosis in SARS-CoV-infected Vero E6 cells. Virology **327:**169-174.
52. **Kato H, Nakajima S, Saito Y, Takahashi S, Katoh R, Kitamura M.** 2011. mTORC1 serves ER stress-triggered apoptosis via selective activation of the IRE1–JNK pathway. Cell Death & Differentiation **19:**310-320.
53. **Kim AH, Khursigara G, Sun X, Franke TF, Chao MV.** 2001. Akt phosphorylates and negatively regulates apoptosis signal-regulating kinase 1. Science Signalling **21:**893.
54. **Kim AH, Yano H, Cho H, Meyer D, Monks B, Margolis B, Birnbaum MJ, Chao MV.** 2002. Akt1 regulates a JNK scaffold during excitotoxic apoptosis. Neuron **35:**697-709.
55. **Sunayama J, Tsuruta F, Masuyama N, Gotoh Y.** 2005. JNK antagonizes Akt-mediated survival signals by phosphorylating 14-3-3. The Journal of cell biology **170:**295-304.
56. **Szegezdi E, Logue SE, Gorman AM, Samali A.** 2006. Mediators of endoplasmic reticulum stress-induced apoptosis. EMBO Rep **7:**880-885.

Figure legends

Figure 1

Activation of the IRE1α-XBP1 pathway by IBV infection.

(a) IBV infection causes ER stress and partially activates the IRE1α-XBP1 pathway in H1299 cells can Vero cells. H1299 cells (left) or Vero cells (right) were infected with IBV (MOI~2) or incubated with UV-IBV and harvested at indicated time points. As a positive control, H1299 cells were treated with 2 mM DTT for 2 hours. Total RNA was extracted and subjected to RT-PCR using primer pairs specific for the indicated genes. The PCR products were resolved using 1% agarose gel electrophoresis, except for XBP1u/XBP1s, where 4% agarose gel was used. The band intensities of HERPUD1, IRE1α, Total XBP1, EDEM1 and ERdj4 were determined by densitometry and normalized to the intensities of corresponding GAPDH bands. Percentage of XBP1 splicing [XBP1s (%)] was calculated as the intensity of XBP1s divided by the total intensities of XBP1u and XBP1s. The experiment was repeated three times with similar results and the result of one representative experiment is shown. Asterisks indicate significant differences between the indicated samples and the 0 hpi sample (*, $P<0.05$; **, $P<0.01$).

(b) H1299 cells and Vero cells were infected with IBV or mock infected for 20 hours, or treated with DTT as in (a). Total RNA was extracted and subjected to real time RT-PCR analysis. Fold inductions of specific genes were calculated using GAPDH as internal references and normalized to the mock infected samples. The experiment was repeated three times with similar results and the result of one representative experiment is shown. Asterisks indicate significant differences between the indicated samples and the mock-treated sample (*, $P<0.05$; **, $P<0.01$).

Figure 2

Effects of IRE1α- and XBP1-knockdown on the activation of the IRE1α-XBP1 pathway

747 (a) H1299 cells were transfected with siEGFP, siIRE1α or siXBP1 before treated with 2mM
748 DTT or mock-treated with same volume of solvent control for 2 hours. Total RNA was
749 extracted and subjected to real time RT-PCR analysis. Fold induction of specific genes were
750 calculated using GAPDH as internal references and normalized to the siEGFP transfected
751 mock-treated sample. The experiment was repeated three times with similar results and the
752 result of one representative experiment is shown. Asterisks indicate significant differences
753 between the indicated samples and the siEGFP transfected samples of the same treatment (*,
754 $P<0.05$; **, $P<0.01$).
755 (b) H1299 cells were transfected with siRNAs before infected with IBV (MOI~2) for 20 hours.
756 Total RNA extraction, real time RT-PCR and data analysis were performed as in (a). The
757 experiment was repeated three times with similar results and the result of one representative
758 experiment is shown. Asterisks indicate significant differences between the indicated samples
759 and the siEGFP transfected sample (**, $P<0.01$).

760 **Figure 3**

761 **Effects of IRE1α- and XBP1-knockdown on IBV-induced apoptosis**

762 (c) Effects of IRE1α- and XBP1-knockdown on IBV-induced PARP cleavage. H1299 cells in
763 duplicate were transfected with siIRE1α, siXBP1 or siEGFP. At 48 hours post transfection,
764 cells were infected with IBV (MOI~2) or mock infected. One set of cells were harvested at
765 the indicated time points and subjected to western blot analysis using antibodies against
766 IRE1α, XBP1, IBV N and PARP respectively. β-tubulin was included as loading control.
767 Percentage of PARP cleavage [PARP Clv. (%)] was calculated as the intensity of cleaved
768 PARP [PARP(Cl)] divided by the total intensities of full length PARP [PARP(FL)] and
769 PARP(Cl). In the second set of cells, total RNA was extracted and subjected to RT-PCR
770 using primers specific for XBP1 and GAPDH.
771 (d) Quantification of PARP cleavage in siRNA transfected cells infected with IBV. Percentage of
772 PARP cleavage in cells transfected with siIRE1α, siXBP1 or siEGFP and infected with IBV

773 for 22 hours was determined as in (a). The bar chart shows results from three independent
774 experiments and indicates standard deviations and p values.
775 (e) Effects of IRE1α- and XBP1-knockdown on IBV-induced caspase activation. The IBV-
776 infected, 22 hpi protein samples and the siEGFP-transfected mock infected protein sample
777 from (a) were subjected to Western blot analysis using antibodies against IBV N, caspase 8,
778 caspase 3 and caspase 9 respectively. β-actin was included as loading control. Percentage of
779 caspase cleavage was calculated as the intensity of cleaved caspase divided by the total
780 intensities of full length and cleaved caspase.
781 (f) The culture supernatants from IBV-infected samples in (a) were clarified by centrifugation
782 and subjected to plaque assay analysis using confluent monolayer of Vero cells. Virus titers
783 were expressed as the logarithm of plaque forming units (PFU) per ml of supernatants. The
784 experiment was repeated three times with similar results and the result of one representative
785 experiment is shown.
786 **Figure 4**
787 **Overexpression of full-length IRE1α protects cells from IBV-induced apoptosis**
788 (a) H1299 cells were transfected with pcDNA3.1-IRE1α-HA or pcDNA3.1. At 24 hours post
789 transfection, cells were infected with IBV (MOI~2) or mock infected. Cells were harvested at
790 indicated time points and subjected to western blot analysis using antibodies against HA-tag,
791 IBV N and PARP. β-actin was included as loading control. Percentage of PARP cleavage
792 was calculated as in Figure 3a.
793 (b) Quantification of PARP cleavage in plasmid transfected cells infected with IBV. Percentage
794 of PARP cleavage in cells transfected with pcDNA3.1 or pcDNA3.1-IRE1α-HA and infected
795 with IBV for 24 hours was determined as in (a). The bar chart shows results from three
796 independent experiments and indicates standard deviations and p values.

797 (c) Schematic diagrams showing the functional domains of IRE1 protein. A lysine to alanine
798 mutation at K599 results in loss of IRE1 kinase activity. The RNase domain of IRE1 is
799 deleted to generate the ΔRNase mutant. TM, transmembrane domain.
800 (d) H1299 cells were transfected with pcDNA3.1-IRE1α -HA, pcDNA3.1-IRE1α-K599A-HA,
801 pcDNA3.1-IRE1α-ΔRNase-HA or pcDNA3.1 in duplicate. At 24 hours post transfection,
802 cells were infected or mock infected as in (a). In one set of the cells, western blot analysis
803 was performed as in (a). In the second set of cells, total RNA was extracted and subjected to
804 RT-PCR using primers specific for XBP1, ERdj4 and GAPDH. The experiment was repeated
805 three times with similar results and the result of one representative experiment is shown.
806 Asterisks indicate significant differences between the indicated samples and the pcDNA3.1
807 transfected 24 hpi sample (**, P<0.01).

808 **Figure 5**

809 **Overexpression of XBP1s, but not XBP1u, protects cells from IBV-induced apoptosis**

810 (a) H1299 cells were transfected with pEGFP-C1, pEGFP-XBP1u or pEGFP-XBP1s in duplicate.
811 At 24 hours post transfection, cells were infected with IBV (MOI~2) or mock infected. Cells
812 were harvested at indicated time points and subjected to western blot analysis using
813 antibodies against EGFP, IBV N and PARP. β-actin was included as loading control.
814 Percentage of PARP cleavage was calculated as in Figure 3a. In the second set of cells, total
815 RNA was extracted and subjected to RT-PCR using primers specific for ERdj4, IBV genomic
816 RNA and GAPDH.
817 (b) Quantification of PARP cleavage in plasmid transfected cells infected with IBV. Percentage
818 of PARP cleavage in cells transfected with pEGFP-C1, pEGFP-XBP1u or pEGFP-XBP1s,
819 and infected with IBV for 24 hours was determined as in (a). The bar chart shows results
820 from three independent experiments and indicates standard deviations and p values.

(c) Schematic diagrams showing the functional domains of XBP1u, XBP1s and XBP1-DN. All three proteins contain the bZIP DNA binding domain. The proteasome degradation motif in XBP1u is deleted to generate the dominant negative XBP1-DN.

(d) H1299 cells were transfected with pXJ40-FLAG or pXJ40-FLAG-XBP1-DN. At 24 hours post transfection, cells were infected with IBV (MOI~2) or mock infected. Cells were harvested at indicated time points and subjected to western blot analysis using antibodies against FLAG-tag, IBV N and PARP. β-actin was included as loading control. Percentage of PARP cleavage was calculated as in Figure 3a.

(e) Quantification of PARP cleavage in plasmid transfected cells infected with IBV. Percentage of PARP cleavage in cells transfected with pXJ40-FLAG or pXJ40-FLAG-XBP1-DN, and infected with IBV for 24 hours was determined as in (d). The bar chart shows results from three independent experiments and indicates standard deviations and p values.

Figure 6

JNK and Akt are involved in the anti-apoptotic function of IRE1α

(c) JNK hyperphosphorylation and Akt hypophosphorylation in IRE1-knockdown cells infected with IBV. H1299 cells were transfected with siIRE1 or non-target siRNA before infected with IBV and harvested at the indicated time points. Western blot analysis was performed using antibodies against IRE1α, IBV N, PARP, phos-JNK, total JNK, phos-Akt and total Akt. β-actin was included as loading control. Percentage of PARP cleavage was calculated as in Figure 3a. Percentages of JNK or Akt phosphorylation were calculated as the band intensities of phosphorylated JNK or phosphorylated Akt divided by the band intensities of the corresponding total JNK or total Akt respectively. The experiment was repeated three times with similar results and the result of one representative experiment is shown. Asterisks indicate significant differences between the indicated samples and the siNC transfected samples of the same time point (*, $P<0.05$; **, $P<0.01$).

(d) Akt protects cells from IBV-induced apoptosis. H1299 cells were transfected with pcDNA3.1 or pcDNA3.1-myr-AKT1. At 24 hours post transfection, cells were infected with IBV (MOI~2) or mock infected. Cells were harvested at indicated time points and subjected to western blot analysis using antibodies against IBV N, PARP, phos-Akt and total Akt. β-actin was included as loading control. Percentage of PARP cleavage was calculated as in Figure 3a. The experiment was repeated three times with similar results and the result of one representative experiment is shown. Asterisks indicate significant differences between the indicated samples and the pcDNA3.1 transfected samples of the same time point (**, $P<0.01$).

(e) JNK is required for IBV-induced apoptosis. H1299 cells were transfected with siJNK1/2 or siEGFP before infected with IBV or mock infected. Cells were harvested at indicated time points and subjected to western blot analysis using antibodies against IBV N, PARP, phos-JNK and total JNK. β-actin was included as loading control. Percentage of PARP cleavage was calculated as in Figure 3a. The experiment was repeated three times with similar results and the result of one representative experiment is shown. Asterisks indicate significant differences between the indicated samples and the siEGFP transfected samples of the same time point (*, $P<0.05$; **, $P<0.01$).

Figure 7

Working model

IBV infection induces ER stress and activation of IRE1α-XBP1 pathway of the UPR. Downstream UPR genes such as ERdj4 and P58IPK were induced to resolve the ER stress. IRE1 protect IBV-infected cells from apoptosis by: 1) converting the pro-apoptotic XBP1u to anti-apoptotic XBP1s; 2) suppressing the pro-apoptotic kinase JNK and 3) promoting the anti-apoptotic kinase Akt.

Fig 1

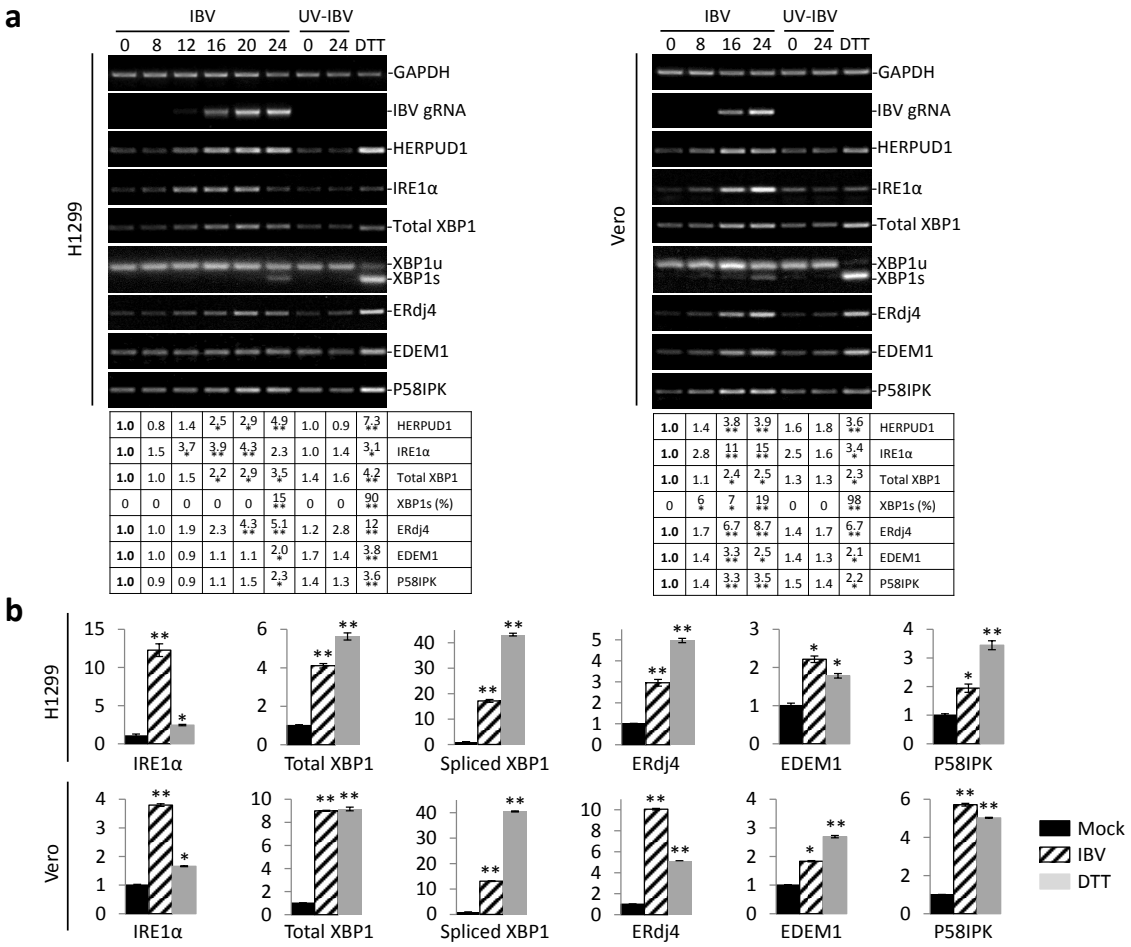

1.0	0.8	1.4	2.5 *	2.9 *	4.9 **	1.0	0.9	7.3 **	HERPUD1
1.0	1.5	3.7 *	3.9 **	4.3 **	2.3	1.0	1.4	3.1 *	IRE1α
1.0	1.0	1.5	2.2 *	2.9 *	3.5 *	1.4	1.6	4.2 **	Total XBP1
0	0	0	0	0	15 **	0	0	90 **	XBP1s (%)
1.0	1.0	1.9	2.3	4.3 **	5.1 **	1.2	2.8	12 **	ERdj4
1.0	1.0	0.9	1.1	1.1	2.0 *	1.7	1.4	3.8 **	EDEM1
1.0	0.9	0.9	1.1	1.5	2.3 *	1.4	1.3	3.6 **	P58IPK

1.0	1.4	3.8 **	3.9 **	1.6	1.8	3.6 **	HERPUD1
1.0	2.8	11 **	15 **	2.5	1.6	3.4 *	IRE1α
1.0	1.1	2.4 *	2.5 *	1.3	1.3	2.3 *	Total XBP1
0	6 *	7 *	19 **	0	0	98 **	XBP1s (%)
1.0	1.7	6.7 **	8.7 **	1.4	1.7	6.7 **	ERdj4
1.0	1.4	3.3 **	2.5 *	1.4	1.3	2.1 *	EDEM1
1.0	1.4	3.3 **	3.5 **	1.5	1.4	2.2 *	P58IPK

Fig 2

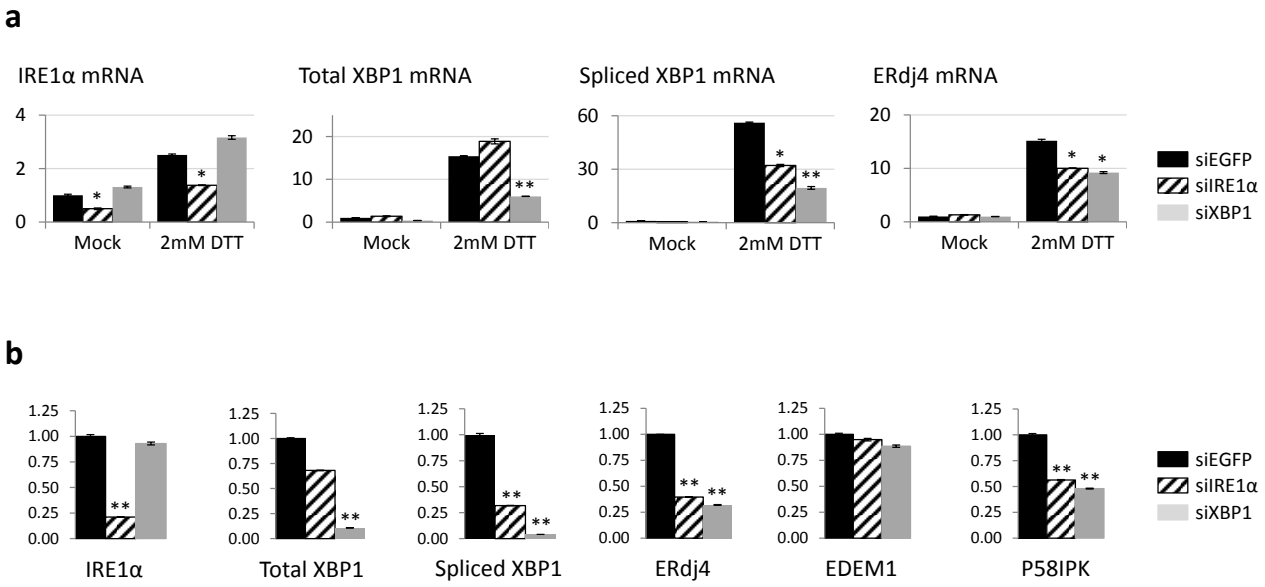

Fig 3

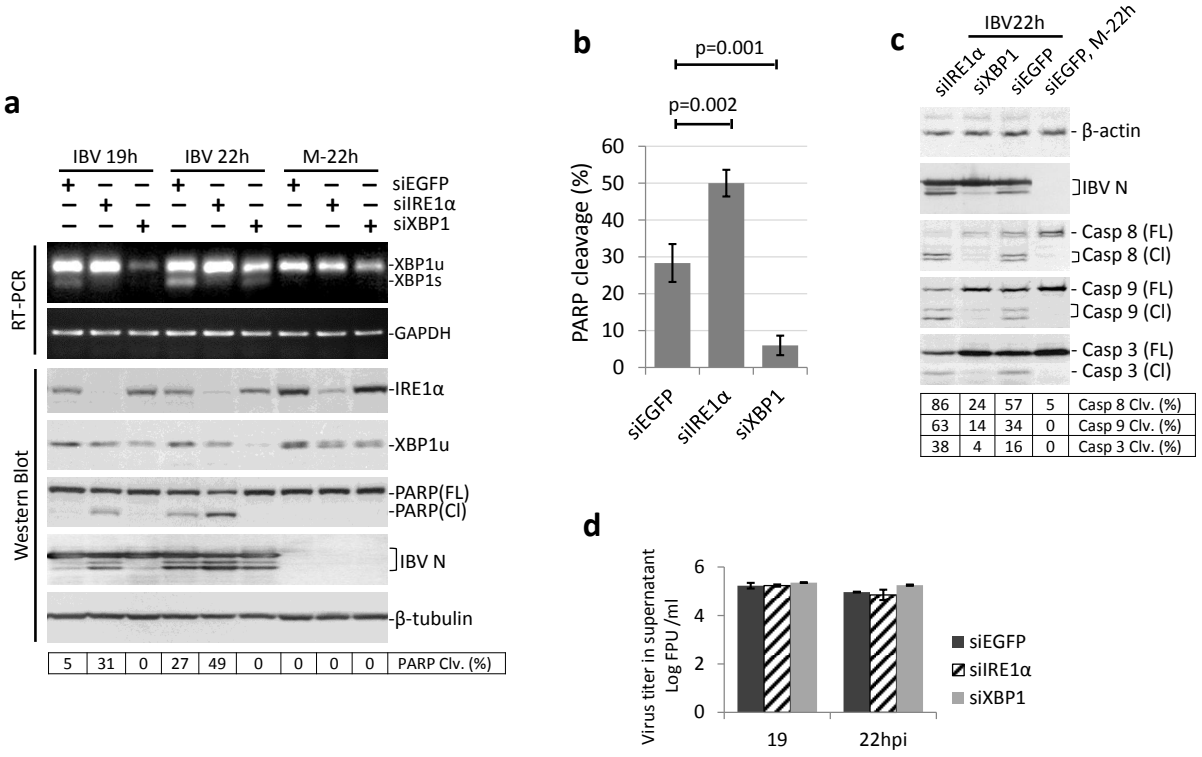

Fig 4

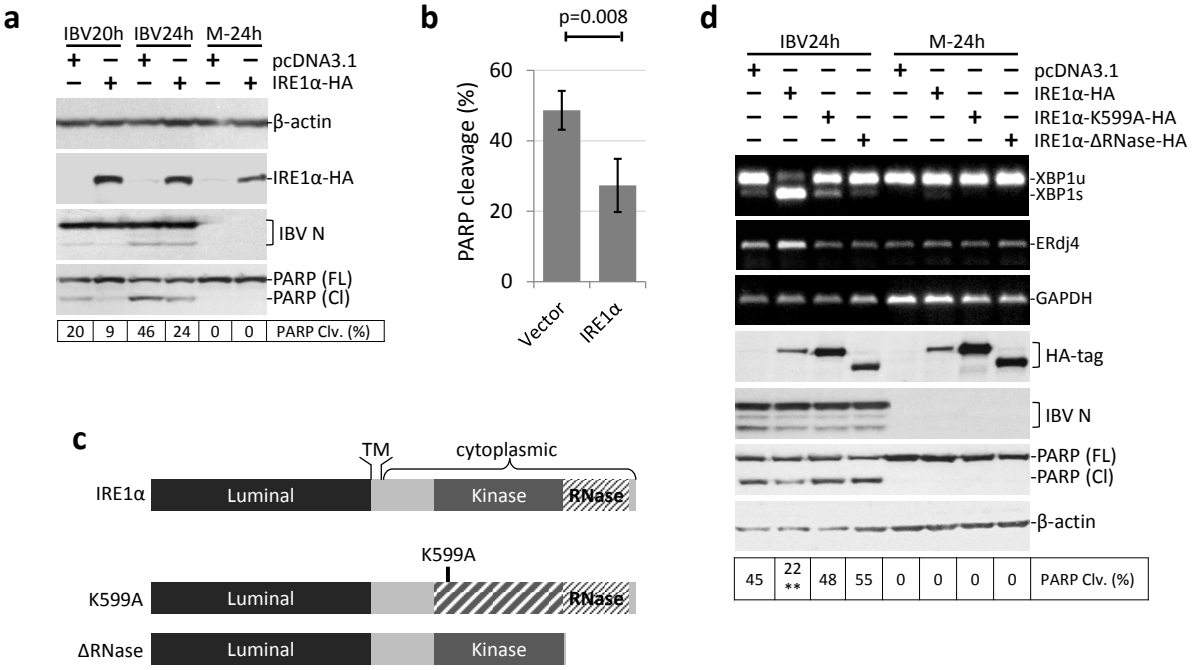

Fig 5

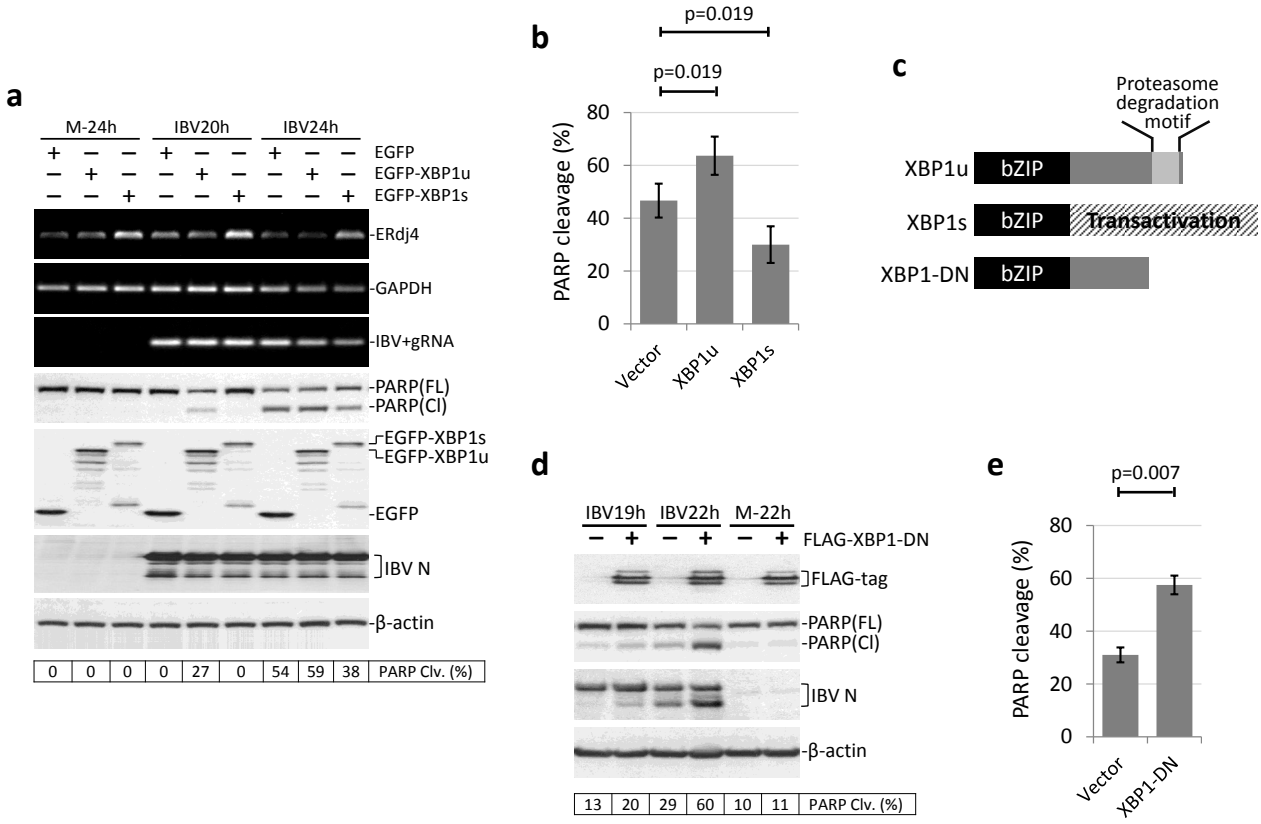

Fig 6

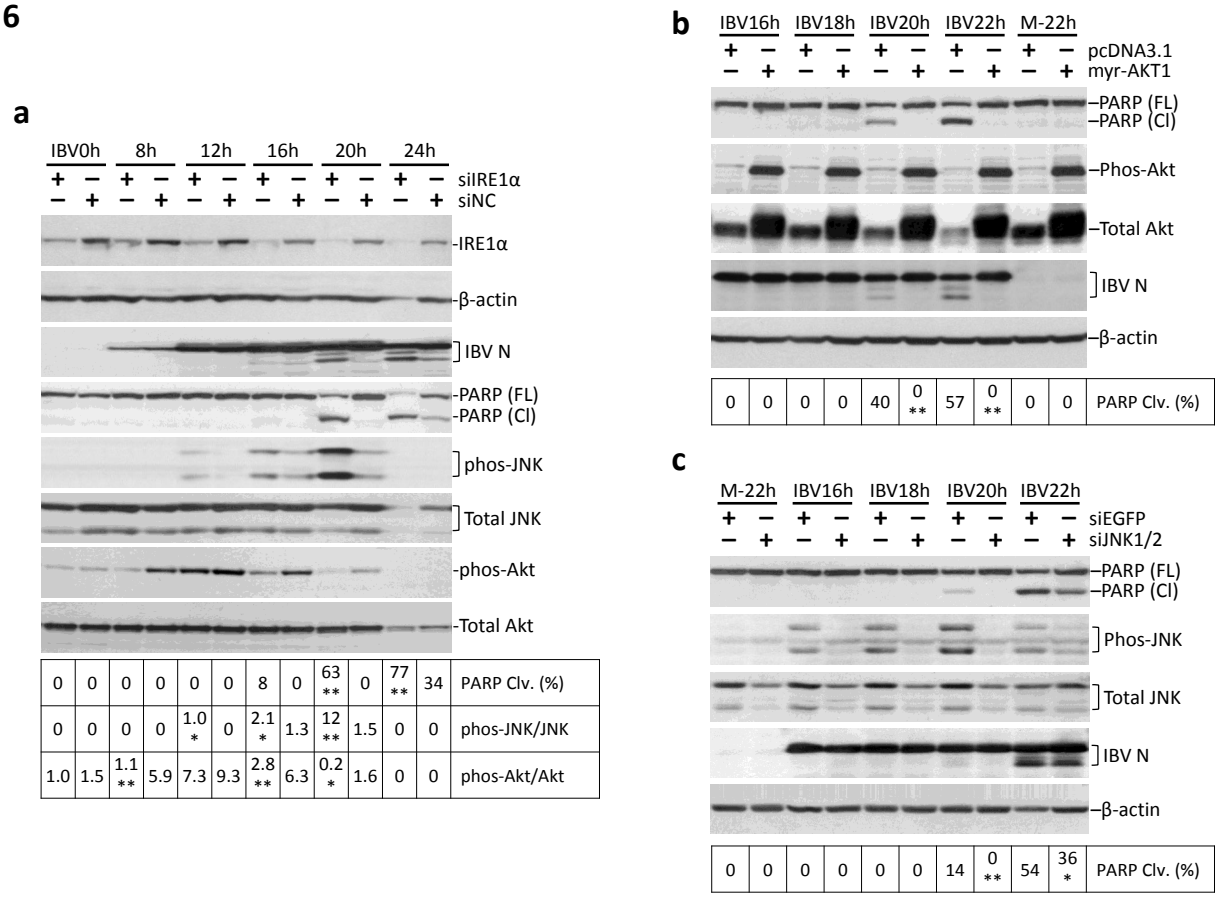

0	0	0	0	0	0	8	0	63 **	0	77 **	34	PARP Clv. (%)
0	0	0	0	1.0 *	0	2.1 *	1.3	12 **	1.5	0	0	phos-JNK/JNK
1.0	1.5	1.1 **	5.9	7.3	9.3	2.8 **	6.3	0.2 *	1.6	0	0	phos-Akt/Akt

0	0	0	0	40	0 **	57	0 **	0	0	PARP Clv. (%)

0	0	0	0	0	0	14	0 **	54	36 *	PARP Clv. (%)

Fig 7